Size-independent fcc-to-icosahedral structural transition in unsupported silver clusters: An electron diffraction study of clusters produced by inert-gas aggregation

D. Reinhard*
Institut de Physique Expérimentale, EPFL, 1015 Lausanne, Switzerland

B. D. Hall
Department of Physics, Massey University, Palmerston North, New Zealand

D. Ugarte
Laboratório Nacional de Luz Síncrotron, Caixa Postal 6192, Campinas 13081-970 São Paolo, Brazil

R. Monot†
Institut de Physique Expérimentale, EPFL, 1015 Lausanne, Switzerland

(Received 12 August 1996)

The structure of free silver clusters, produced in an inert-gas-aggregation source and flowing in a molecular beam has been studied by electron diffraction. Large clusters (up to 11 nm in diameter) of both icosahedral and fcc structure are observed. Cluster structure is investigated as a function of evaporation temperature and molecular weight of the inert gas in the source. An increase in evaporation temperature leads to increasing formation of fcc particles in the beam, without a significant change in particle size. The existence of large icosahedra is ascribed to the formation of metastable structures, grown under conditions dominated by kinetic factors. Furthermore, these large icosahedra show pronounced relaxation, indicating that they are subject to significant internal strain. This strain appears to be accommodated by deformation of the lattice, rather than by the inclusion of defects. The diffraction findings are supported by transmission-electron-microscopy measurements made on samples taken from the beam. [S0163-1829(97)02812-9]

I. INTRODUCTION

Since the first observations of icosahedral and decahedral structures in small gold particles three decades ago,[1] there has been considerable interest in the growth and stability of nanometer-sized atomic clusters. It is now recognized that a cluster's atomic arrangement may be different from that of the bulk crystal, provided that the energy cost of internal strain is offset by a favorable arrangement of surface atoms. The interplay of surface and volume contributions to a cluster's total energy implies that one structure will be preferred to others over specific size ranges. For example, silver clusters smaller than about 5 nm are expected to adopt an icosahedral structure; clusters larger than 9 nm, on the other hand, are expected to be face centred cubic (fcc), as in the bulk.[2]

Theoretical studies support these general predictions for a range of materials. Some studies have used elasticity theory and have applied bulk parameters to model nanometer-sized clusters.[2,3] Others have used molecular-dynamics computer simulations, and a suitable approximation to the interatomic potential, to investigate stable cluster forms and particle dynamics at finite temperature.[4–8] All these studies have shown that when there is a size-dependent change to the equilibrium structure, the energy differences between competing forms is small. Only slight modifications to the details of surface faceting are sufficient to favor one structure type over another.[9]

Experimental observations of small particle structures are numerous (see Ref. 10 for a recent review). Both electron diffraction and electron microscopy [especially high-resolution electron microscopy (HREM)] on supported samples have provided a wealth of structural information and document the occurrence of icosahedra and decahedra in many metals. Also of interest are HREM observations of the structural rearrangement of clusters in real time under the influence of an intense electron beam. In this behavior, referred to as ''quasimelting,'' a cluster changes rapidly between a range of structures known to be in competition at small sizes.[11,12]

Electron diffraction on unsupported particles is a technique that has been developed by various groups.[13,14] In the study of rare gases, the technique has been very successfully coupled with molecular-dynamics simulations. The structure, dynamics, and temperature of small rare-gas clusters has been deduced from a series of experiments.[15] However, in spite of these studies, the transition from icosahedral to fcc structure, which must occur as clusters grow in size, is a topic of current speculation.[16]

HREM studies routinely observe *large* metal clusters with icosahedral or decahedral morphology. In many cases, specific contrasts show that these are, in fact, multiple-domain fcc particles: the strain inherent in the icosahedral or decahedral structure (noncrystallographic atomic arrangements, implying the presence of axes of fivefold symmetry) is relieved by inclusion of defects, such as dislocations or stacking faults.[10,17] In other cases, it has been possible to show that large metal clusters actually have icosahedral or decahedral *structure*, characteristic of stable configurations predicted at smaller sizes.[18] These belong to the class of multiply twinned particles (MTPs), in which the strain associated

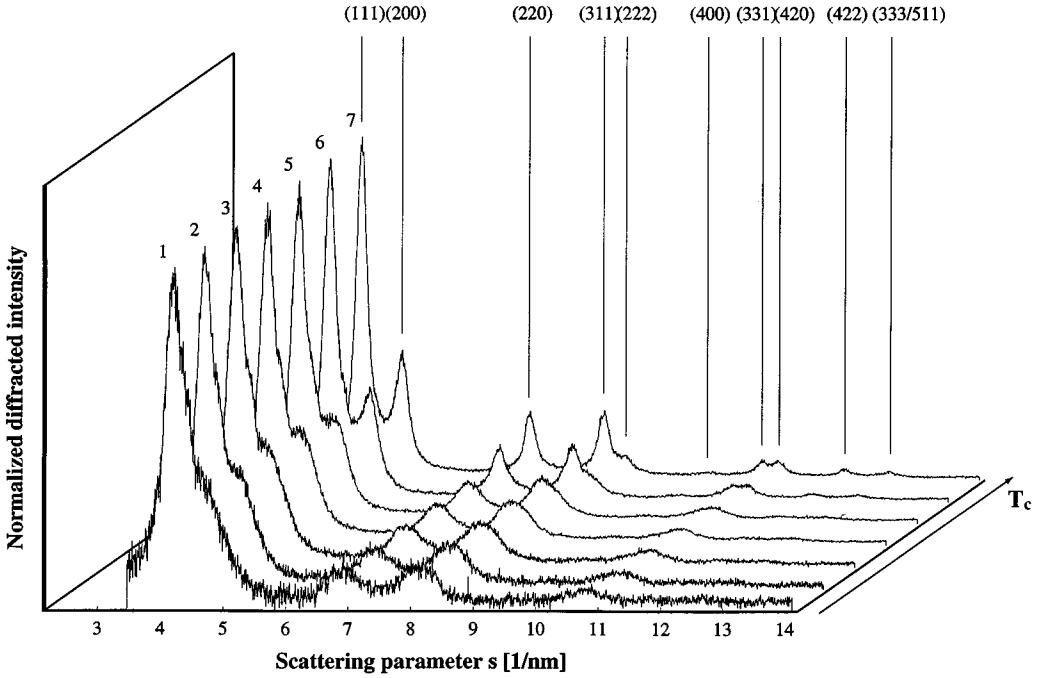

FIG. 1. Diffraction patterns obtained from Ag clusters in a molecular beam of He gas. The seven profiles are taken at increasing values of evaporation temperature (coolest in front, warmest at the back). The numbers associated with each curve indicate the order in which the measurements were made; they are the same numbers used in Table I, where the experimental conditions are recorded. The intensities of the curves have been normalized so that all have the same height at the first maximum, $s \approx 4.2$ nm^{-1}. The positions of the Bragg reflections for bulk silver are indicated by Miller indices on profile 7.

with the fivefold symmetry is accommodated by elastic deformation of the constituent tetrahedral domains. It has been suggested that these particles are evidence that conditions of growth, as opposed to purely thermodynamical considerations, can determine the final atomic arrangement.[10] If the growth of a particular structure can continue well beyond the size at which another form becomes energetically favorable, the size of the particle, due to the increasingly complex rearrangements that would have to occur, becomes an obstacle to a structural change and the cluster remains set in its atomic arrangement. The energy barrier that must be overcome in order to change structure is not known. It has been proposed that for a Lennard-Jones potential, clusters larger than about 10^4 atoms will require an energy in excess of the latent heat of fusion.[19] In the case of smaller particles, quasimelting observations suggest that the energy required is below the melting point, however, the quasimelting phenomenon is not well understood and may well result from rapid melting-solidification events, unresolved in electron microscope studies.[20]

In this study we report observations of large (up to 11-nm diameter) free silver clusters produced by the inert-gas-aggregation technique and flowing in a molecular beam. We show that, by varying conditions in the region of nucleation and growth, a gradual, and reproducible, transition between icosahedral and fcc structures is obtained without significant change in particle size. We argue that these observations can be understood in terms of conditions imposed by the kinetics of particle growth that are compatible with our understanding of the inert-gas-aggregation technique.

The study is principally based on *in situ* electron-diffraction measurements performed on clusters in the molecular beam, although we have also removed samples from the beam and observed these with both conventional and high-resolution electron microscopy. This diffraction technique has several advantages over observations made on supported samples by HREM, or other techniques. First, the clusters are completely isolated in the molecular beam. This removes any ambiguity regarding cluster-substrate interactions whose effect on cluster structure is not well known. Second, the measurement *in situ* under high-vacuum conditions minimizes the possible contamination of a cluster's surface by impurities, which could interfere with the fine energy balance of the particle by affecting the surface energy. Third, interactions between the electron beam and clusters do not lead to excitation of the clusters, as they can do in HREM,[21] because of the very short exposure time as clusters cross the electron beam. Finally, diffraction on the randomly oriented clusters in the beam provides an ensemble average of the structures present. It is therefore possible to obtain an objective measure of the distribution of structures within a sample and how this evolves when source conditions are varied.

The following section briefly describes the experimental apparatus and the conditions under which measurements were made. Two series of measurements are then presented to show the dependence of particle structure on source conditions. These results are analyzed by comparing data with calculated diffraction patterns based on model structures. This enables the constituent structures to be identified as well as their relative abundance and sizes estimated. We then discuss our findings in terms of the process of cluster growth in an inert-gas-aggregation source.

TABLE I. The experimental conditions corresponding to the experimental measurements in Fig. 1. T_{ev} is the evaporation temperature, P_V is the metallic vapor pressure obtained from Ref. 51, and P_{He} is the inert-gas pressure in the nucleation chamber.

Expt. no.	1	2	3	4	5	6	7
T_{ev} (°C)	1260±2	1281±2	1291±2	1301±2	1311±2	1352±2	1402±2
P_{He} (mbar)	3.2±0.1	3.2±0.1	3.2±0.1	3.2±0.1	3.2±0.1	3.2±0.1	3.2±0.1
P_V (mbar)	0.5±0.05	0.73±0.05	0.80±0.06	0.93±0.06	1.07±0.07	1.6±0.2	2.9±0.3

II. EXPERIMENTAL APPARATUS

A detailed description of the complete electron diffraction apparatus has been published previously[22] and only details relevant to this study are given here.

Cluster nucleation and growth take place in a cylindrical stainless steel chamber (diameter 87 mm, length 110 mm) the walls of which are kept cool by water circulating at 14 °C. An evaporation source is placed in the middle of the chamber. The source is comprised of a graphite crucible around which a tungsten filament is wound. This unit is inserted into an arrangement of radiation shields made from tantalum foil and a thermocouple is lodged in the base of the crucible, from the side, to monitor the evaporation temperature and also to allow closed-loop temperature control (±2° at 1600 °C). The silver to be evaporated is placed in the graphite crucible (silver of 99.99% purity was used throughout), and an inert gas (He, or Ar, both of 99.9999% purity, or a He/Ar mixture) is injected at room temperature through a large orifice (diameter: 8 mm) in the rear of the chamber.

A molecular beam is generated by two stages of differential pumping between the nucleation chamber and the diffraction chamber. At each stage, the inert gas, seeded with clusters of silver, is pumped through a small orifice into a chamber at lower pressure. This has the effect of refining the mass ratio of clusters to gas at each stage, by selectively pumping away a higher proportion of carrier gas. It also creates a well-directed molecular beam that serves as the sample for diffraction.

Upon entry to the diffraction chamber, the molecular beam is crossed at right angles by a beam of high-energy electrons (100 kV). The resulting Debye-Scherrer diffraction pattern is measured along a diameter by a pair of charge-coupled device detectors located at the bottom of the chamber. Downstream from the beam crossing, a mechanism is inserted in the molecular beam that is capable of rapidly exposing electron microscope slides to the cluster flux. This allows samples to be taken during an experiment. They are later removed from the vacuum and transferred to an electron microscope (Philips EM430-ST) for study.

III. EXPERIMENTAL METHOD, RESULTS, AND ANALYSIS

Two series of measurements are presented in this paper. The first was made by keeping the pressure of He constant in the nucleation chamber while the temperature of the evaporation source was progressively increased. The other series was made at roughly constant evaporation temperature, and nucleation chamber pressure, while the composition of the carrier gas was varied by mixing together Ar and He. In that way, two parameters affecting nucleation have been investigated. In this section, diffraction patterns for both series are presented, as well as the results of electron microscope analyses of two samples extracted from the beams. We then describe the method used to analyze the diffraction data, which involves matching the experimental profiles with combinations of calculated diffraction patterns for model structures, and the results of that analysis are presented.

A. Measurements with increasing evaporation temperature

A series of seven diffraction patterns was obtained under conditions of constant He gas pressure (3.2 mbar) in the nucleation chamber. The profiles are shown in Fig. 1 and the parameters associated with these measurements are listed in Table I.

In Fig. 1, the experimental profiles are presented in a perspective plot format, with the coolest evaporation temperature (1260 °C) in the foreground and the hottest (1402 °C) in the background. The profiles have been corrected for background scattering, due to carrier gas, and normalized to have the same height at the maximum of the profile ($s \approx 4.2$ nm^{-1}). The locations of Bragg diffraction peaks for bulk silver at 300 K are also shown, labeled by Miller indices.

The general features of the series are well defined: from 1 to 7 the profiles become less noisy (no smoothing has been applied to the data), which is an indication of an increasingly strong cluster signal. Hence with increasing evaporation temperature, the number of clusters produced is increasing. It is apparent that features in the diffraction profiles are increasingly sharp from 1 to 7. In profile 7 these features agree well with the position of fcc diffraction peaks. Careful inspection

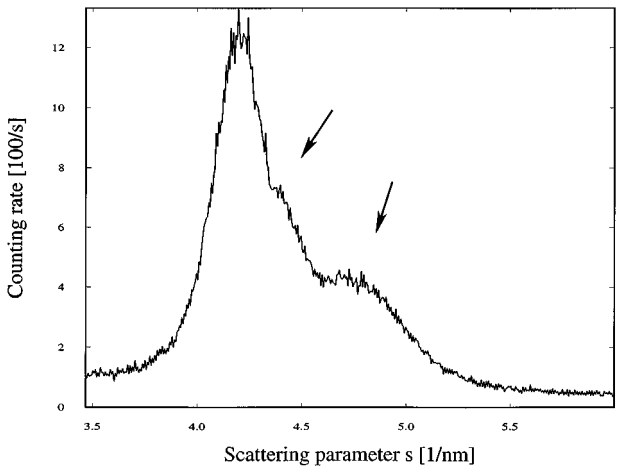

FIG. 2. A detailed view of diffraction profile 4 showing two distinct features on the right of the peak maximum. The shoulder at $s \approx 4.4$ nm^{-1} is an indication of the presence of large icosahedra in the sample.

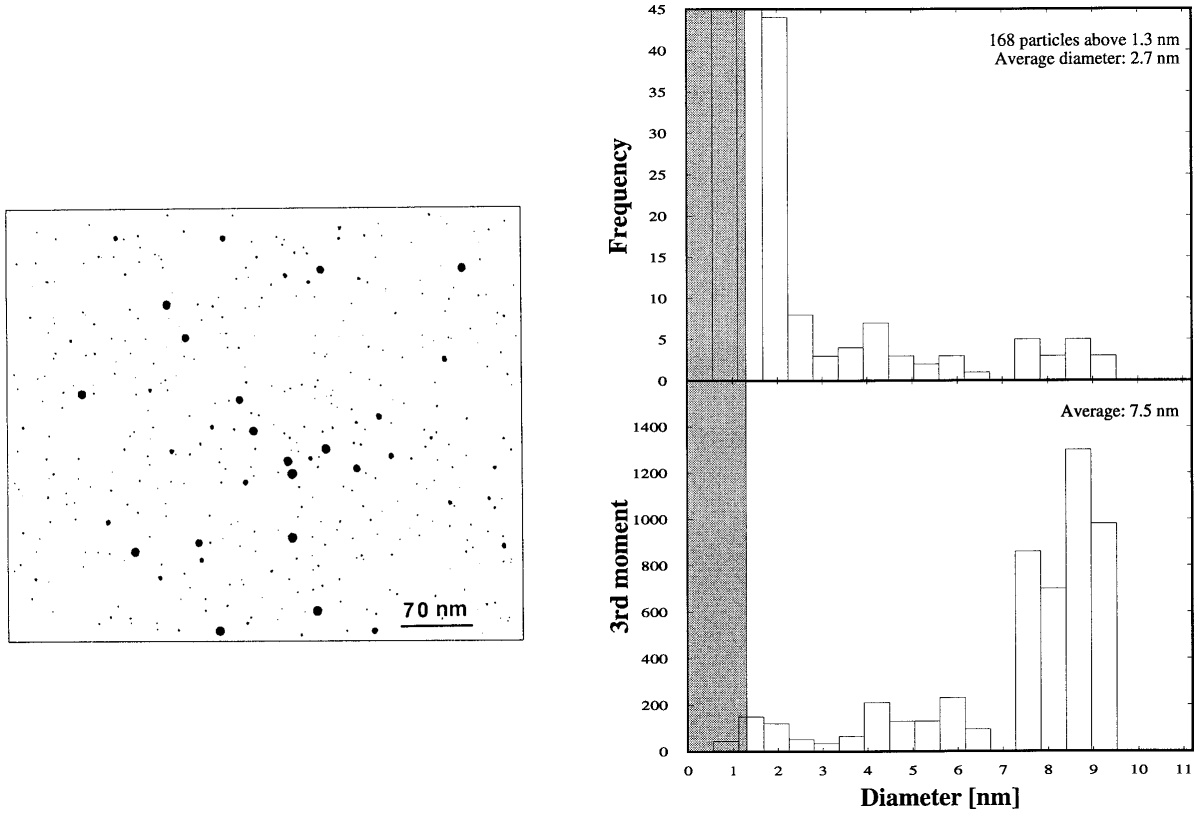

FIG. 3. Binary image and size distributions obtained from the supported sample corresponding to profile 7 (Ag/He; see also Fig. 1 and Table I). The gray regions indicate the limits of uncertainty due to noise in the images treated.

of the strong composite peak in the region $s \in [3.5,5]$ nm^{-1} shows two things: firstly, a developing shoulder at $s \approx 4.7$ nm^{-1} that separates into a peak in profiles 6 and 7. Secondly, a less marked shoulder at $s \approx 4.4$ nm^{-1}. This feature is of importance to later analysis and is discussed in Appendix A. It effectively identifies the presence of large icosahedral clusters in the beam. Figure 2 shows the region of interest in more detail, taken from the experimental profile 4.

Of the small particle samples taken from the beam, we have selected one, corresponding to profile number 7 (the highest evaporation temperature in the series), for presentation here. An analysis of the cluster size distribution is shown in Fig. 3. Histograms show the frequency of the apparent cluster diameters, and the volume-weighted frequency (third moment), which is proportional to the intensity of the diffraction pattern from the clusters. The binary image (after discrimination of particle contours against the background) in which a particle appears as a uniformly dark surface against a white background is also shown.

HREM has been performed on the same sample and a selection of images are given in Fig. 4. Overall, a large number of small particles (diameter $\leqslant 3$ nm) were observed, mostly difficult to classify according to structure, due to unfavorable observation conditions or irregular atomic arrangement. In this size range some fcc particles [see Figs. 4(a) and 4(b)] and some decahedra were observed. At intermediate sizes (3 nm$<$diameter$<$5 nm) several decahedra and icosahedra were observed. The larger particles in the sample had diameters between 7 and 10 nm. These particles, because of their volume, dominate in a diffraction measurement. Their structures were seen to be multiple-domain fcc clusters [see Figs. 4(c) and 4(d)].

B. Measurements with varying inert-gas composition

A series of six diffraction patterns have been obtained under conditions of constant inert-gas pressure (3.2 mbar), while varying the inert-gas composition progressively between pure He and pure Ar. The measurements were made at approximately the same temperatures although taken from two different experimental runs. The diffraction patterns are shown in Fig. 5 and the experimental conditions are summarized in Table II. As before, the profiles are presented in a perspective format. In this case, two profiles with pure He gas are in the foreground and the proportion of Ar gas is increased towards the background.

Similar features and tendencies to Fig. 1 can be identified in Fig. 5. Once again the two shoulders to the maximum of the profile can be clearly seen. The shoulder at $s \approx 4.7$ nm^{-1} again develops into a peak in profile 13. The lesser shoulder, at $s \approx 4.4$ nm^{-1}, is apparent in profiles 8 through 12. Note, however, profile 13, obtained with pure Ar, does not show clear fcc diffraction peaks compared with profile 7 of Fig. 1.

The results of a statistical analysis of cluster sizes, obtained from a supported sample corresponding to profile 9 is shown in Fig. 6 (particles in this sample were produced by condensation in pure He). Histograms of the diameter distribution and of the volume-weighted frequency (third moment) are shown, as well as the binary image used to obtain these statistics. HREM images of a selection of clusters from this sample are shown in Fig. 7. They show two, clearly identifiable, icosahedral clusters [Figs. 7(b) and 7(c)] and one decahedral cluster [Fig. 7(a)]. These images are typical of those clusters that could be identified in this sample (see Ref. 23 for a discussion of HREM identification of small particle structures).

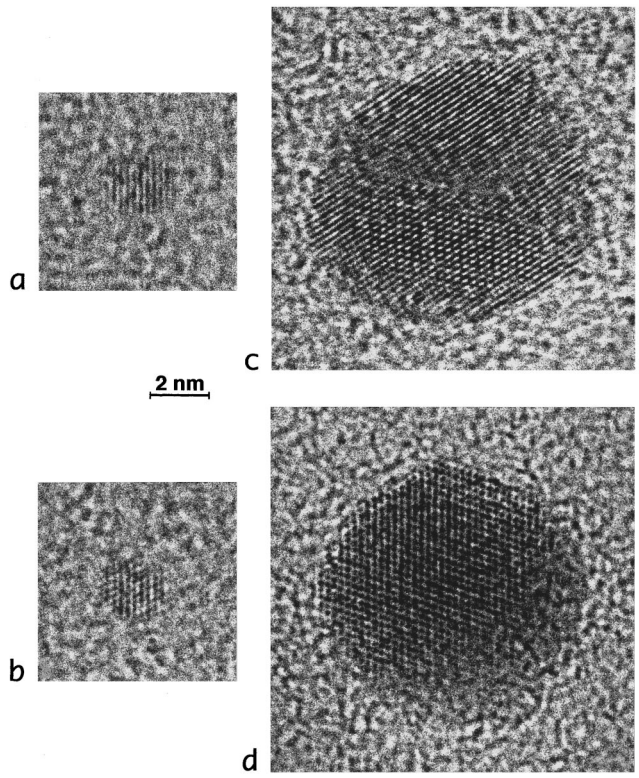

FIG. 4. HREM pictures obtained from the supported sample corresponding to profile 7 (Ag/He see also Fig. 1 and Table I). (a) fcc crystal with one family of (111) planes resolved, diameter 3 nm; (b) fcc crystal observed along the [110] zone axis, diameter 2.6 nm; (c) cluster with several fcc domains, diameter 10.3 nm; (d) fcc crystal observed along the [110] zone axis, diameter 8.7 nm.

As in the case of profile 7, a large number of smaller clusters were present (diameter $\leqslant$2.5 nm) and their structures could not readily be identified. For larger sizes (between 3 and 8 nm) monodomain fcc particles were absent and fcc particles consisting of several domains were rare. It is striking that the particles observed were almost all icosahedra (see Fig. 8), as was the largest particle observed [see Fig. 7(c)]. Most particles were remarkably well formed, showing well-developed facets and quasispherical shapes [see Figs. 7(a) and 7(b)].

C. Calculated diffraction patterns

Because there is quite definitely a range of cluster sizes in the molecular beam, and more than one type of structure can be present, the experimental data must be considered to represent a superposition of diffraction patterns from a variety of clusters. In earlier work, we showed that information about the composition and size ranges of clusters in the beam can be extracted by using a computer to fit a weighted combination of calculated diffraction patterns to the experimental data.[24] In this study, a variation of that technique has been adopted, requiring operator intervention, rather than an automatic procedure. The need for this is the result of inadequate structure models for the large icosahedra (see Appendix A): important relaxation occurs in the atomic positions of the larger silver clusters which gives rise to differences between the diffraction profiles of the relaxed structure and those calculated using the Mackay geometry.[25] While the Mackay model diffraction patterns reproduce the main features of the larger icosahedra, they cannot be relied upon for automatic fitting. Furthermore, dynamic diffraction effects significantly alter the peak intensities of large clusters, especially fcc particles.[26]

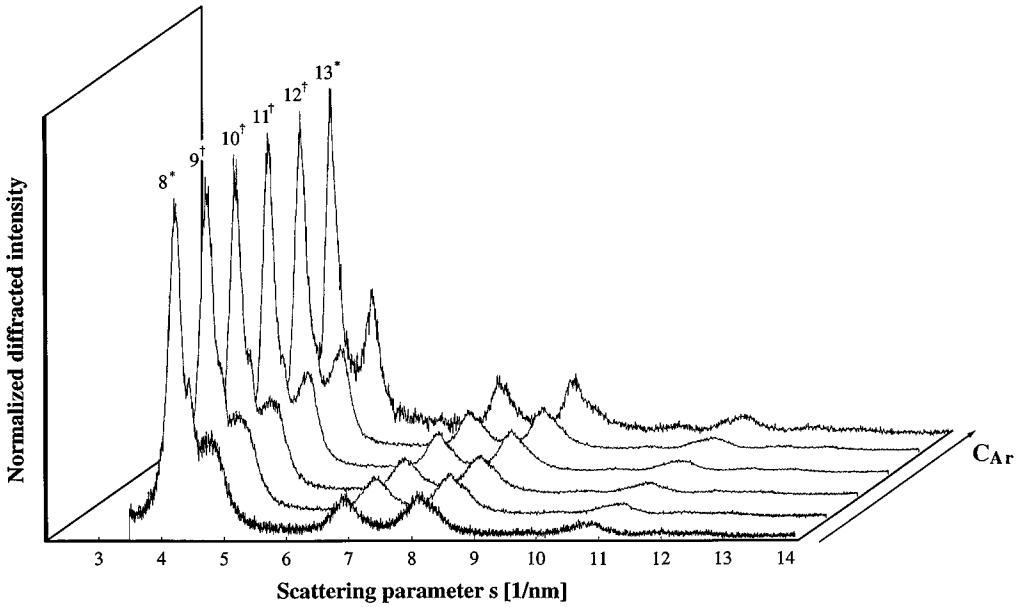

FIG. 5. Diffraction patterns obtained from Ag clusters in a molecular beam of a mixture of He and Ar gas. The seven profiles are taken with an increasing proportion of Ar in the composition (the two patterns in the front correspond to pure He, pure Ar at the back). The numbers associated with each curve are used in Table II, where the experimental conditions are recorded. The data were obtained during two experimental runs: the symbols $*$ and † indicate sets of measurements made together. The intensities of the curves have been normalized so that the first maximum, at $s \approx 4.2$ nm^{-1}, has the same height.

TABLE II. The experimental conditions corresponding to the experimental measurements in Fig. 5. T_{ev} is the evaporation temperature, the corresponding metal vapor pressure is approximately $P_V=0.6$ mbar at the lower temperatures, and $P_V=0.8$ mbar for profiles 11 and 12 (Ref. 51). ''Proportion Ar'' is the percentage of Ar gas mixed with He and introduced to the nucleation chamber at 3.2 mbar. The symbols $*$ and † represent group measurements made during the same experiment.

Expt. no.	8*	9†	10†	11†	12†	13*
T_{ev} (°C)	1267±2	1268±2	1268±2	1288±5	1286±5	1268±2
Proportion Ar (%)	0	0	10	20	30	100

Debye-Scherrer diffraction patterns are calculated by assuming a particular form for a model cluster and applying the Debye formula of kinematical diffraction theory to obtain a profile of diffracted intensity. The Debye equation calculates the scattering cross section for an ensemble of atoms, averaged over all orientations, expressed as

$$I_{\mathrm{kin}}(s)=I_0 N f^2(s)\left(1+\frac{D}{N}\sum_{n\neq m}\frac{\sin(2\pi s r_{mn})}{2\pi s r_{mn}}\right). \quad (1)$$

I_0 is the intensity of the incident beam and $I_{\mathrm{kin}}(s)$ is the number of electrons scattered per unit solid angle per unit time in the direction defined by s.[27] The scattering parameter s is given by $s=2\sin(\theta)/\lambda$, where θ is half the scattering angle and λ is the electron wavelength. The quantity $f(s)$ is the atomic scattering factor (we are assuming clusters of a single type of atom) and is available in tabulated form.[28] N is the number of atoms in the cluster and r_{mn} is the distance separating atom m from atom n. The Debye-Waller factor D is included to express the attenuation of the interference term in the Debye equation, caused by thermal vibrations. A simple model assumes that the displacement of atoms is random and isotropic about their equilibrium positions. In this case,

$$D=\exp[-(2\pi s\Delta x)^2], \quad (2)$$

where Δx is the rms atomic displacement from equilibrium along a Cartesian coordinate. Evaluation of the Debye equation for very large clusters is done using an efficient algorithm based on the fast Fourier transform, rather than by direct computation of Eq. (1).[29]

We have used three structure types in our cluster models: face-centered-cubic, decahedral, and icosahedral. The fcc clusters were constructed using the bulk lattice parameter at 300 K for silver, and represent complete outer-shell growth sequences of a cuboctahedron with regular triangular facets in the ⟨111⟩ directions. The icosahedral structure, in terms of close-packing of spheres, has been described by Mackay[25] and the decahedral structure by Bagley;[30] we have used the nearest-neighbor distances in our models proposed by Ino, in which the structures are homogeneously relaxed according to

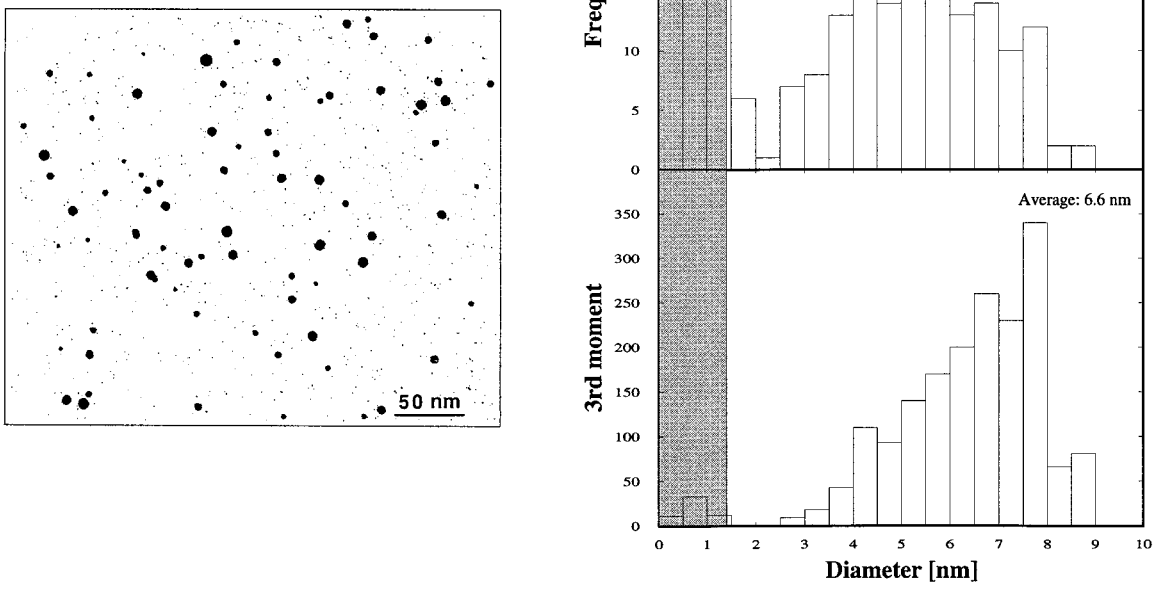

FIG. 6. Binary image and size distributions obtained from the supported sample corresponding to profile 9 (Ag/He; see also Fig. 5 and Table II). The gray regions indicate the limits of uncertainty due to noise in the images treated.

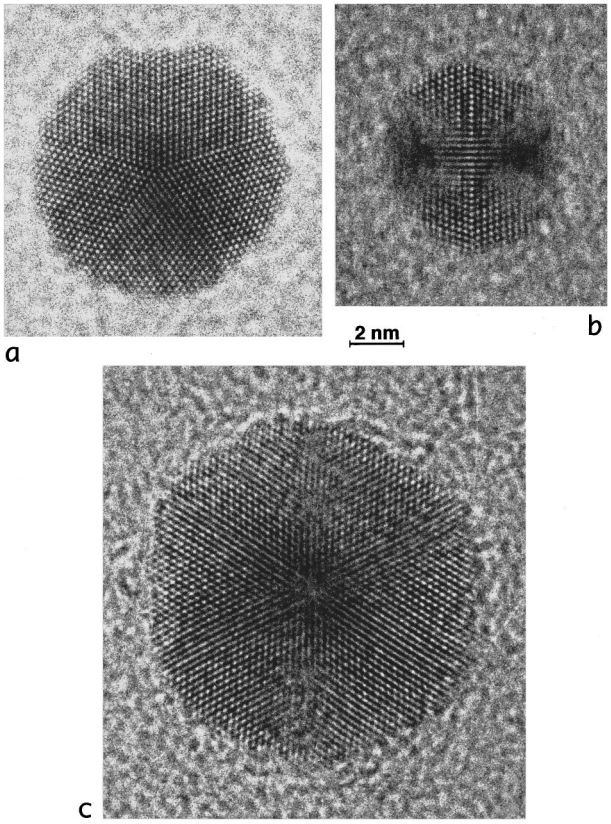

FIG. 7. HREM pictures obtained from the supported sample corresponding to profile 9 (Ag/He; see also Fig. 5 and Table II). (a) Decahedral particle observed along the axis of fivefold symmetry, diameter 9.9 nm; (b) icosahedral particle observed close to an axis of twofold symmetry, diameter 7.3 nm; (c) icosahedral particle observed close to an axis of threefold symmetry, diameter 13.6 nm.

the elastic constants of bulk silver.[3] The decahedral models are truncated by five (100) planes, parallel to the fivefold symmetry axis, as described by Ino.[3]

D. Fitting of calculated diffraction patterns to experimental data

Clearly, there is a broad range of cluster sizes present in the molecular beam and each cluster size will contribute a distinct character to the overall diffraction pattern. Size effects in the diffraction patterns of nanometer-sized clusters are important, as are the differences between the patterns obtained from icosahedra, on the one hand, and decahedra or fcc, on the other. The differences between diffraction features associated with the latter two are less pronounced, especially if the fcc clusters are imperfect. Therefore, electron diffraction is well suited to the identification of icosahedral clusters and can make an estimation of their size. In considering our method of analysis, two points should be borne in mind: first, the scattered intensity of a diffraction pattern increases in proportion to the number of atoms within the cluster. Hence, when a distribution of sizes is broad (e.g., Fig. 3) the dominant contribution to the diffraction pattern will come from the larger cluster sizes. This is the reason for reporting the third moment of the size distributions in our supported samples (Figs. 3 and 6), which indicates the relative contribution by a given size of particle to the total integrated intensity of the diffraction pattern. Two, diffraction patterns obtained from a cluster with inhomogeneous structure are, to a first approximation, characteristic of the individual domains of coherent structure within the particle.

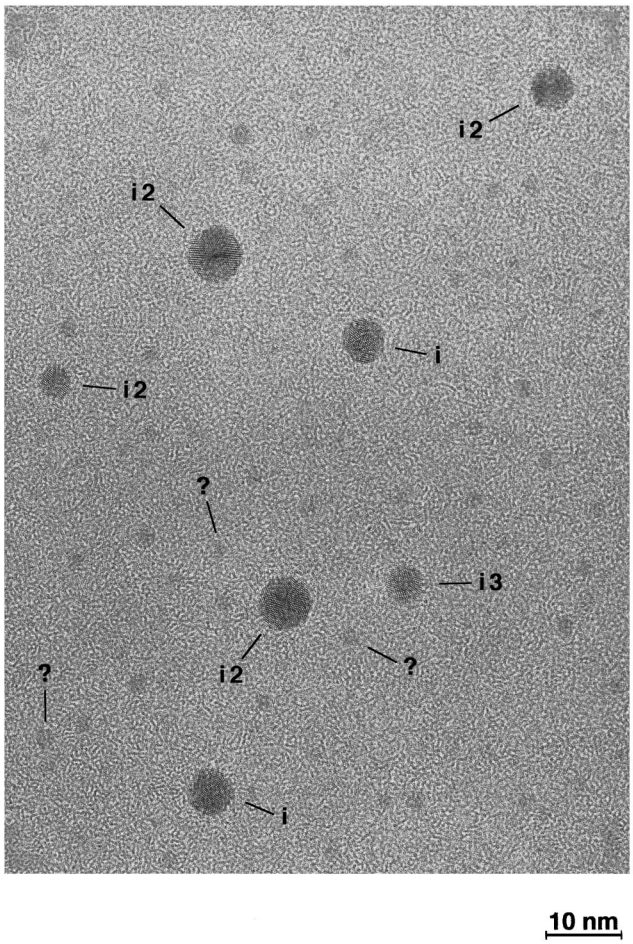

FIG. 8. A HREM picture obtained from the supported sample corresponding to profile 9 (Ag/He; see also Fig. 5 and Table II). A majority of small particles (diameter $\leqslant$2.5 nm) is visible, some of which, marked with a ''?,'' could be fcc. All the larger particles can be identified as icosahedra. Labeling for these is $i2$ when viewed close to an axis of twofold symmetry, $i3$ when viewed close to an axis of threefold symmetry, and i when viewed with some other orientation.

A collection of model cluster diffraction patterns has been built up to cover a range of sizes from 13 to 86 000 atoms per cluster. This gives a total of 29 calculated profiles per structure type (of which there are three). To compare these calculations with the experimental data we take a Gaussian distribution function to describe the size distribution for each structure type. Thus our distribution function can be written as

$$f_i(D_{ij}) = \alpha_i \exp\left[-\frac{(D_{ij}-\mu_i)^2}{2\sigma^2} \right], \tag{3}$$

where $f_i(D_{ij})$ is the size distribution for one of the three structure types ($i=1,2,3$), D_{ij} is the diameter of the jth cluster in the series of structure type i, α_i is a positive number representing the relative weight of that distribution in the overall population, μ_i is the mean diameter of the distribu-

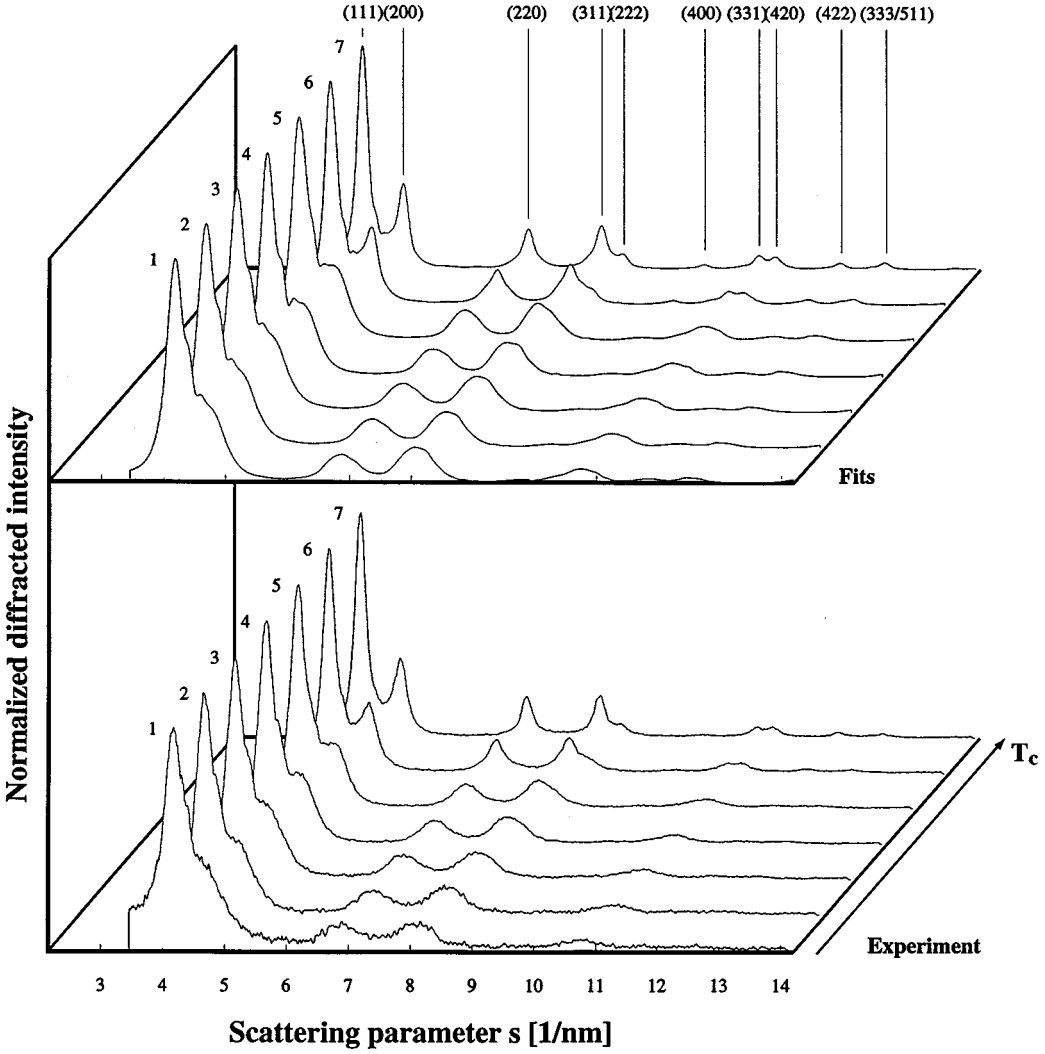

FIG. 9. The results of fitting the experimental data with model particle structures. The data in the lower part of the figure correspond to those in Fig. 1, although they have been smoothed numerically. The upper part of the figure shows the corresponding fits to this data. The numbers 1–7 refer to the data in Table I.

tion, and σ is its standard deviation (assumed to be the same for all three structure types). The parameters α_i, μ_i, σ are adjustable; however, there is an additional constraint on the values of α_i:

$$\sum_{i=1,2,3} \alpha_i = 1, \tag{4}$$

so there are effectively six parameters which can be manipulated to obtain a fit to the experimental data.

The presentation of results in the next section uses the parameter ν_i to indicate the relative contribution of a particular structure type to the total diffracted intensity. It is based on the volume weighted size distribution for a particular structure according to

$$\nu_i = C \sum_{j=1}^{29} f_i(D_{ij}) V_{ij}, \tag{5}$$

where the volume of the model particle is

$$V_{ij} = \frac{\pi}{6} D_{ij}^3 \tag{6}$$

and the normalization constant

$$C = \frac{1}{\Sigma_{i=1}^{3} \Sigma_{j=1}^{29} f_i(D_{ij}) V_{ij}}. \tag{7}$$

E. Analysis

The results of fitting a combination of calculated diffraction profiles to the experimental data are given in Fig. 9 and Table III. The experimental data, shown in smoothed form, correspond to the series in which evaporation temperature was progressively increased (see also Fig. 1 and Table I).

The fitted profiles in Fig. 9 show excellent agreement with the experimental data, also shown in the figure. The calculated profiles are clearly capable of reproducing all of the identifiable features of the experimental curves: the shape and evolution of features in the principal diffraction peak are closely matched, as is the evolution of the peaks at $s \approx 6.9$

TABLE III. Results of fitting experimental data with calculated diffraction profiles. The raw experimental data are displayed in Fig. 1 and the conditions summarized in Table I. The curves obtained by fitting are shown in Fig. 9. The parameter μ represents the mean of the fitted distribution for a particular structure type, α is the relative weight of the structure type in the overall population, and ν is its relative contribution to the total diffracted intensity.

		Expt. no. 1	2	3	4	5	6	7
					T_c (°C)			
		1260±2	1281±2	1291±2	1301±2	1311±2	1352±2	1402±2
Cubo.	μ (nm)	6.0	6.0	6.0	6.0	6.0	6.0	6.0
	α	0.003	0.003	0.003	0.003	0.003	0.060	0.200
	ν (%)	3.3	3.3	3.3	1.3	1.6	22.4	45.2
Ico.	μ (nm)	6.9	6.9	6.9	7.4	7.9	9.8	9.8
	α	0.020	0.020	0.020	0.050	0.020	0.015	0.015
	ν (%)	39.3	39.3	39.3	46.6	28.2	22.2	15.1
Deca.	μ (nm)	2.0	2.0	2.0	2.7	2.7	2.7	3.2
	α	0.977	0.977	0.977	0.947	0.977	0.925	0.785
	ν (%)	57.4	57.4	57.4	52.1	70.2	55.4	39.7
σ (nm)		0.6	0.6	0.6	0.6	1.0	1.7	1.7

and 8.1 nm^{-1} and the appearance of fcc reflections in profile 7. As to the uniqueness of the fits presented, we are confident that larger particles dominating a particular sample are unambiguously identified by the procedure. There is no way by which, for instance, profile 7 could have been fitted satisfactorily without a dominant fcc contribution, or, profile 4, without a significant contribution from large icosahedra. There is, however, ambiguity with regard to the smaller particle contributions to a fit, particularly decahedra. This is discussed further below.

The data displayed in Table III identify some trends within the series of measurements. First, there is a significant component of large icosahedra in each measurement. The average size, μ, appears to increase steadily with increasing temperature, and the proportion, α, of icosahedra with respect to other structures passes through a maximum at profile 4 (T_{ev}=1300 °C).

Second, a large number of decahedra are included in all fits. They are always very small in size and it should be remembered that the contribution of these clusters to the total scattering is in proportion to their volume; consequently their relative contribution to the overall profile, ν, is considerably less than the relative abundance α suggests. Furthermore, their presence in the fit does not necessarily signal that of decahedral clusters in the sample. Earlier studies have suggested that small decahedra may well be included because their diffraction mimics the effects of imperfections in fcc clusters. The decahedral contribution to the profiles in this study is necessary to change the shape of certain features: increasing the width at the base of the main diffraction peak and rounding the peaks at $s \approx 6.9$ and 8.1 nm^{-1}.

The qualitative nature of the fitting procedure makes it difficult to assign uncertainties to the entries in Table III. Errors will depend on the values of μ and σ, and to some extent on the structural family (due to the presence of distinctive feature in the diffraction profiles). Generally, the larger the values of μ and σ, the stronger the constraint on α thereby reducing the uncertainty in it. We estimate a typical uncertainty of 10% in α, and for μ and σ somewhat higher than this.

The high-resolution microscopy performed on the supported sample associated with profiles 7 and 9 (see Secs. III A and III B) supports the findings above. In particular, Fig. 8 confirms the abundance of small particles (diameter $\leqslant$2.5 nm) and the predominantly icosahedral structure of the larger particles found for profile 4, very similar to profile 9 to which Fig. 8 is associated.

Similar results have been obtained as a result of fitting the data in which the gas composition was varied. In this case, however, a satisfactory fit to experimental profile 13 (see Fig. 5) could not be obtained: the asymmetric triangular shape of the peaks at $s \approx 6.9$ and 8.1 nm^{-1} could not be reproduced; nor could the absence of most fcc reflections when the pronounced peak at $s \approx 4.7$ nm^{-1} was present.

IV. DISCUSSION

There is evidence in the observations reported above that the large icosahedra forming in these experiments are not simply a manifestation of ''size effects,'' favoring the icosahedral structure over fcc. Indeed, we have noted that in fits to the experimental profiles, and in the electron microscopy performed on supported samples, a significant number of very small clusters are present. The structure of these clusters, albeit difficult to identify, is clearly not dominated by icosahedra, which are easily recognized by HREM. This is significant because theories of cluster stability predict the icosahedron to be the most stable atomic configuration for the smallest sized particles. In the present study, on the contrary, we observe only large icosahedra. We also note that, as the conditions of nucleation and growth are changed, we are able to change the composition of the cluster beam so that fcc particles form and are essentially comparable in size, or smaller than, the large icosahedra previously present.

These observations can be satisfactorily explained in

terms of what is known about the processes of nucleation and growth in an inert-gas-aggregation source. A discussion of the conditions within such a source and their effects on the growth of small particles is given in Appendix B.

The formation of large particles occurs in a region some distance from the evaporation source, where there is a discontinuity in the rate of cooling of the metal vapor caused by strong convection currents. At this ''inner front,'' the very rapid drop in temperature of the metallic vapor enhances supersaturation and a high rate of nucleation occurs. Metallic vapor density in this region is high and particle growth proceeds rapidly. Particles also form from the dense vapor closer to the evaporation source; however, the temperature there is relatively high and growth is slower due to reevaporation, resulting in a large number of small particles. The observations of the present study show fairly distinct particle populations, which can reasonably be attributed to the growth of particles in different zones within the source. The additional gas flow, caused by extracting the gas through the orifice at one end of the source, conceivably acts only as a perturbation to the flow patterns set up by convection near the hot evaporation source: the associated zones of nucleation and growth may distort, but the processes occurring within are unlikely to be substantially changed. The mixture of particles and gas being pumped into the diffraction chamber contains clusters from the different zones within the source.

It is significant that the large icosahedra described here could only be obtained by tuning source conditions to relatively high values of helium pressure and evaporation temperature.[31] The region of formation and growth for the largest particles will be one in which vapor density is high and temperature relatively low; it is reasonable therefore to consider the structure of these large particles as being determined by growth rates, rather than purely energetic considerations. Atoms sticking to a particle tend to build on the initial structure. Although there has been some discussion about the exact sequence of how this may occur,[10,32–38] it is clear that as the size of the particle increases, the energy required for it to undergo full internal structure rearrangements also increases. Thus, while small clusters may fluctuate rapidly between various structures at a particular temperature, larger clusters will do so more slowly, or not at all, depending on the activation barrier to a structural change. Particle growth combined with a rapidly falling probability for structural change suggests that the particle structure is being effectively quenched, and eventually frozen, in a form that would not occur under conditions of slower growth, close to thermodynamic equilibrium. As already suggested by Marks, the final structure then reflects the relative stability of competing structures at much smaller sizes, before the size-related activation barrier prevented further rearrangements.[10] The large particles actually observed are in a metastable state.

When the temperature of the evaporation source is varied, causing the composition of the molecular beam to change, we observe a change in structure from icosahedral to fcc while the size of these particles remains roughly the same. This size independence of particle formation in the ''intermediate zone'' has already been reported (see Appendix B). The change to fcc structure when the temperature is sufficiently high may be attributed to an increase in the temperature within the intermediate zone. A higher temperature could allow larger particles to undergo structural rearrangement before their structure is frozen in, or it may reflect the temperature dependence of the surface tension, which becomes isotropic with increasing temperature, thus discounting the surface energy gain of the icosahedron and favoring the fcc structure.[11]

The measurements made by varying the molecular weight of the inert gas are more complicated to interpret. The effect of any buffer gas molecules is to remove heat from the vapor atoms via collisions. Argon gas should be more effective than helium at cooling the metallic vapor,[39] in spite of presenting a smaller cross section, allowing the metal vapor to diffuse farther from the evaporation source.[40] We therefore expect that the vapor density increases away from the evaporation source and that cooling is enhanced closer to the source. Unlike the situation above, this now suggests that growth occurs in an increasingly cool region, rich in metallic vapor, hence an environment in which the nucleation and growth rates are increasingly high. This might be expected to favor icosahedral growth, rather than oppose it. However, we believe that a possible explanation lies in the increasing importance of growth by coalescence of clusters. It is well known that cluster coalescence is a growth process that can occur in the inert-gas-aggregation method.[41] Indeed, HREM micrographs of silver particles collected in previous experiments have shown large numbers of composite clusters, in which domains of icosahedral, decahedral, or fcc structure can be identified. The relative importance of individual growth versus coalescence depends on the density of nucleating clusters. With argon, the enhanced supersaturation leads to a higher rate of formation of cluster nuclei and hence to a higher probability of collision among them. Our inability to find a combination of model structures that could provide a close approximation to the experimental profile 13 supports this hypothesis. Although profile 13 shows some fcc character, the distortions in it are important. In part, these are due to the presence of multiply twinned particles. However, our simple models of these structures are inadequate and it is likely that some more elaborate models, able to account for the complicated structures that occur in composite particles, would help to resolve the discrepancy.

V. CONCLUSION

This study has shown that large icosahedra can be grown by homogeneous nucleation from the vapor and attain considerable size. Although energy considerations alone predict a preference for clusters to adopt an fcc structure even at quite small sizes, this does not occur here because of the kinetics of growth in the source. In a dense and cool metallic vapor, an icosahedral particle can quickly grow and attain sizes such that the energy needed to undergo a structural transformation to fcc is prohibitively large. As a result, the particle retains the icosahedral structure. Significantly, a substrate, which might stabilize a nonequilibrium structure via interactions with the particle's surface, is totally absent in these experiments.

We also note that there is clear evidence of relaxation in the atomic positions of the large silver icosahedra compared

to the geometric Mackay structure. Furthermore, these particles cannot be confused with the icosahedral-shaped multiple-domain fcc particles previously reported and extensively studied. In the latter, internal strain is relieved by the appearance of defects. The diffraction patterns in this case would reflect the fcc character of the individual domains within the particle (see Appendix A). In the large icosahedra found in the present work, on the contrary, the strain inherent to this structure is relieved essentially by elastic deformation of the constituent tetrahedral domains.

It is particularly interesting that this work has been able to roughly tune the conditions of particle production so that the beam of particles is either predominantly fcc or icosahedral in structure. Given that many structural studies of small metal clusters are faced with the inevitable coexistence of these fundamental structures, it is interesting to be able to produce a sample dominated by one type of small particle, especially of icosahedra.

APPENDIX A: DIFFRACTION PROFILES FOR LARGE ICOSAHEDRA

Two distinct aspects of the diffraction profiles obtained from large icosahedra require further discussion: Firstly, the appearance of fine structure in profiles that evolves as a function of particle size. The fine structure in icosahedral diffraction patterns, despite being convolved with particle size distributions, provides an important indicator of the presence of icosahedra in a measurement, as well as giving an idea of their size. We have investigated this using models of atomic structure based on the Mackay geometry.

Secondly, we consider how the diffraction profile of a relaxed icosahedron differs from that of the model chosen. It is well known that the atomic positions in an icosahedron are not exactly those described by the Mackay geometry.[8] Strain within the structure gives rise to relaxation, which becomes more important as the size of the cluster increases. Also, the importance of these deformations is greater in icosahedral particles than it is for fcc or decahedral ones. The large icosahedra observed in this study certainly exhibit relaxation; however, for silver, we do not have more sophisticated structural models available to account for this. We discuss the qualitative differences to a diffraction profile that can be expected, by considering results available of molecular-dynamics calculations applied to large copper icosahedra.[45]

1. Diffraction features of large icosahedra: Mackay structure

The icosahedral geometry described by Mackay arises from consideration of the problem of packing hard spheres in the smallest possible volume.[25] The structure obtained can be visualized as an assembly of twenty distorted tetrahedra, each placed with three sides facing neighboring tetrahedra and all sharing a common apex, at the center of the particle. There is no underlying periodic lattice from which the atomic positions of this structure can be generated. Hence one cannot speak of an associated reciprocal lattice, and the concept of Bragg reflections at specific scattering angles does not apply. The constituent tetrahedra do, however, have an underlying periodicity; they have rhombohedral symmetry.[42]

Careful consideration of the Debye equation (1) shows that the number of terms in the summation corresponding to small values of r_{mn} (compared to the dimension of the particle) will outweigh those for which r_{mn} is large. In other words, the average local atomic arrangement will dominate the diffraction pattern. This argument has been demonstrated numerically: in the case of randomly oriented domains in small particles;[43,44] and in the simple twinning of fcc particles.[24] It is for this reason, for example, that it is possible, using electron diffraction, to identify domains of structure within an inhomogeneous particle.

The diffraction patterns of Mackay icosahedra containing less than about 3500 atoms display profiles with features that change in position and intensity as the size of the cluster changes.[24] Above that size, features begin to appear that can be associated with reflections from the rhombohedral domains. As the particle size increases these features become clearer, although size-dependent details continue to be present.

In Fig. 10, two calculated diffraction profiles are shown, one for a 5-nm particle (ten complete atomic layers, 3871 atoms), the other for a 9.8-nm diameter particle (20 complete layers, 28 741 atoms). An arrow to each of these profiles indicates the position of the emerging rhombohedral (111) Bragg reflection. Figure 11 shows the diffraction pattern of a larger particle, 14.1 nm in diameter (29 layers, 85 609 atoms) in which the reflections associated with the rhombohedral structure are indexed with Miller indices.

2. Relaxation in large icosahedra

In diffraction studies, similar to the present, on both silver and copper clusters we have been successful in fitting calculated profiles to the experimental data using an automatic procedure.[24,45] This approach has not been as successful in the present study because the clusters under investigation are much larger and the relaxation therefore more pronounced. We are, however, able to give a qualitative explanation for the deviations that are observed.

In Fig. 12, an automatic fitting algorithm has been applied to the experimental data profile number 4 (see Fig. 1 and Table I), which is the most icosahedral in character among our series of measurements (see Table III). The fit is shown both superimposed on the experimental data and shifted vertically above them, to allow closer scrutiny. While it succeeds in reproducing the general form of the data, and the relative amplitudes of features are correct, the fit does show distinct regions in which significant differences occur between the profiles.

We believe these discrepancies arise because of the relaxation of the Mackay structure in the silver clusters. Indeed, the fitted distribution of model particles is strongly dominated by icosahedra, with a significant contribution to the diffracted intensity coming from particles whose diameter exceeds 7.5 nm. Although no theoretical data are available regarding relaxation in large silver icosahedra, we have been able to study the effects of relaxation in large copper clusters. The diffraction profile for a copper icosahedron 6.9 nm in diameter (10 179 atoms), whose structure has been obtained by molecular-dynamics calculations,[46] has been compared with that from a Mackay icosahedron containing the same number of atoms. This comparison shows that in specific regions of the diffraction pattern differences are apparent. In most cases these tend to ''round'' the details of the

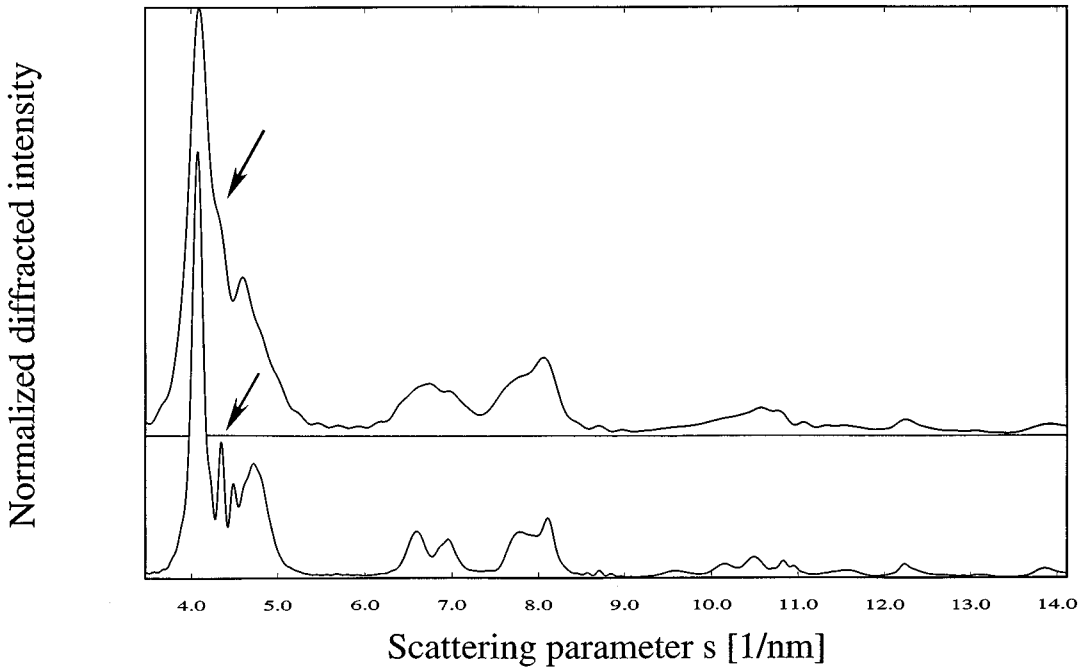

FIG. 10. Diffraction profiles calculated using the Mackay structure for icosahedra containing 3871 atoms (upper curve, particle diameter 5 nm, ten complete layers) and 28 741 atoms (lower curve, particle diameter 9.8 nm, 20 complete layers). The arrows indicate the appearance of a feature associated with the (111) reflection of the rhombohedral lattice.

Mackay pattern, although some enhancement to the detail associated with the rhombohedral (111) reflection from the Mackay structure is observed. In Fig. 12, arrows indicate the parts of the Mackay diffraction pattern that are changed by relaxation. The ''+'' sign indicates an enhancement in the scattering intensity, a ''−'' sign indicates that the Mackay profile will be attenuated. Clearly, relaxation will bring the adjusted profile closer to the experimental one.

To our knowledge, icosahedral structures have been examined for Ni,[7] Ar,[8] Cu,[45] Au,[47] and Pb.[48] The general features of the atomic rearrangements in each case are the same: the central region of the particle is compressed, giving rise to a radial contraction, and a tangential dilation occurs in the outer layers of the structure. There is also a tendency for a convex deformation of the outer facets to occur. It is reasonable to assume that the qualitative changes we observe in the diffraction from a copper cluster be the same as those for a silver cluster. It follows that more accurate models of icosahedral structure would provide a basis for satisfactory automatic fitting of the data. It must be noted that the structure of

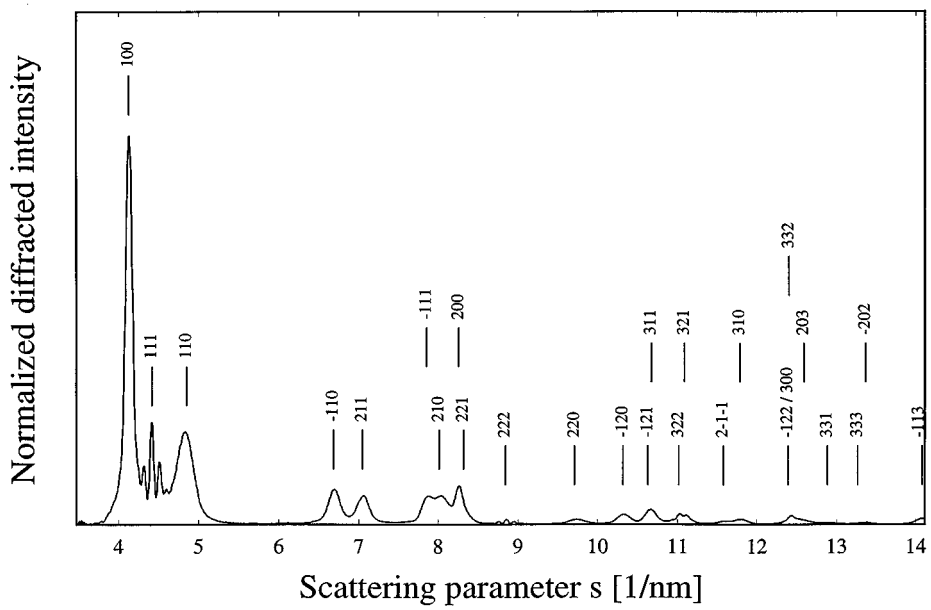

FIG. 11. The diffraction profile for a Mackay icosahedron consisting of 85 609 atoms (29 complete layers, diameter 14.1 nm). The numbers indicate the Miller indices of the diffraction peaks associated with the rhombohedral lattice.

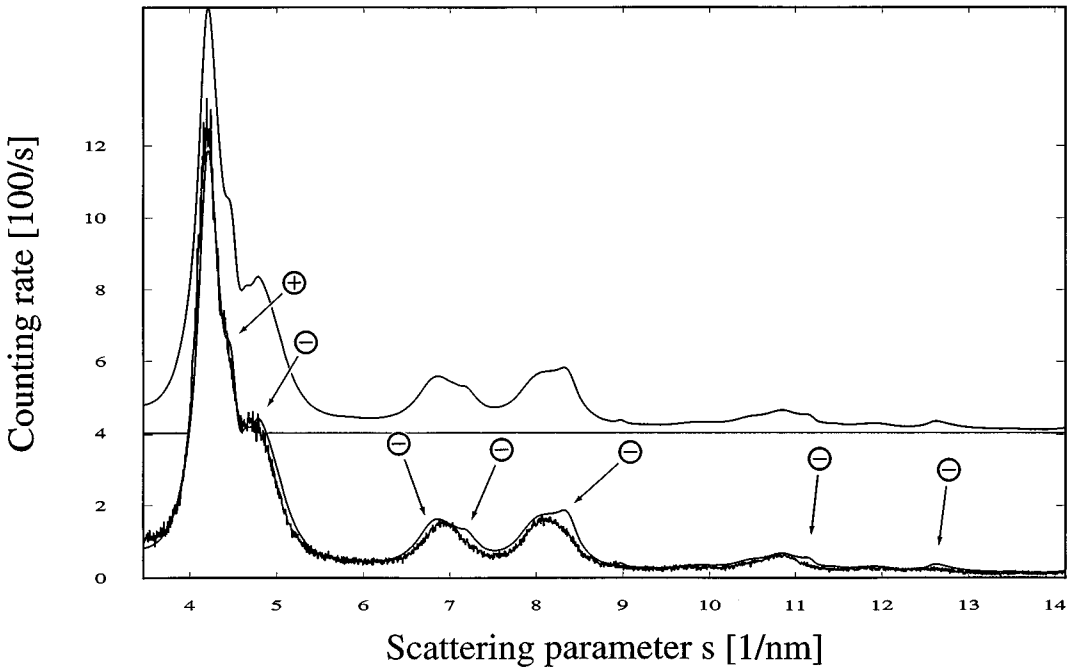

FIG. 12. Illustration of the problems associated with the Mackay icosahedral structure models used in the fitting procedure. The fitted curve is shown twice: superimposed on the experimental curve and shifted upwards, for better visibility. The experimental data correspond to profile 4 (see Fig. 1 and Table I), which has been fitted using an automatic procedure. The + and − signs indicate regions where it is expected that relaxation will enhance (+) or reduce (−) scattering.

the constituent tetrahedra is no longer homogeneous in a relaxed icosahedron. The description given for the Mackay structure therefore no longer applies and the fine structure identified for large icosahedra cannot be interpreted as a rhombohedral (111) Bragg reflection. It is not clear, at present, why this particular feature is nevertheless present, and even enhanced, in the presence of relaxations.

APPENDIX B: NUCLEATION AND GROWTH IN AN INERT-GAS-AGGREGATION SOURCE

Various authors have to some extent described the nucleation and growth of small particles within an inert-gas-aggregation source.[14,39,40,41,49] The most complete description, based on extensive experimental study, has been given by Hayashi *et al.*[40] and Wada.[39] Samples were collected at various distances from an evaporation source, at differing values of inert gas pressure and evaporation temperature, and also with inert gases of different molecular weight. The samples were collected on electron microscope slides and studied using various techniques to determine the crystal habit and structure of the small particles.

In the description offered by Hayashi *et al.* (well illustrated in a paper by Yatsuya *et al.*[50]), a plume of ''smoke'' is observed to extend upwards from the hot evaporation source. Three distinct coaxial zones are identified within this plume; these are associated with changing regimes of convective flow in the vicinity of the source. The zones are named, as follows, the ''inner zone,'' extending directly above the source and horizontally outwards until the ''inner front'' is attained; the ''intermediate zone,'' a thin region, in which strong convective cooling occurs, bounded by the ''inner front'' on the inside and the ''outer zone'' on the outside; the ''outer zone'' extends from the end of the intermediate zone to the limits of the chamber. The actual extent of the zones depends on the evaporation temperature, gas pressure, and gas molecular weight. It should be noted that to move between zones it is necessary to consider a displacement normal to the convective flow, not along the flow, which has considerable extent in the direction of the plume.

The importance of the zones is associated with the experimental finding that particles collected from different zones have distinctly different sizes, as well as distinct habits, depending on conditions of pressure and temperature. Particles from the inner zone are small while a sharp increase in the mass of particles collected occurs in passing through the ''inner front'' to the intermediate zone. Moving through the intermediate zone to the outer zone the particle size diminishes progressively.

The effect of gas pressure is to limit the diffusion of metallic vapor within the zones: lower pressure, by reducing the probability of collision with metal atoms, allows the vapor to extend farther from the evaporation source. The evaporation temperature, being the driving force of the convective flows near the source, affects the distinct nature of the zones described above: at lower temperatures the abrupt change in particle masses between the inner and intermediate zones is attenuated, or is lost entirely. Increasing the temperature has little effect on the sizes of particles that are collected, although their habit tends to change to more rounded, Wulff-like, forms, suggesting growth closer to thermodynamic equilibrium. An interesting remark is made concerning the effect of inert-gas molecular weight: increasing the molecular weight has the effect of increasing the diffusion constant of the metal vapor within the inert gas. As a result, the mass of metal condensing in the inner zone is reduced when the molecular weight of the gas is increased, and the density of the vapor increases in the intermediate zone.

Nucleation and growth of particles is described in the following way. A dense, hot, region of metallic vapor extends outwards from the source, through the inner zone, and encounters strong convective cooling at the base of the intermediate zone (i.e., at the ''inner front''). This gives rise to strong supersaturation, with a high rate of nucleation and growth. A strong gradient of vapor density forms here, enhancing further vapor diffusion to the region. Nucleation and growth are low in the inner zone, compared to the intermediate zone, because of the lower supersaturation and high temperature there. Moving through the intermediate zone, and into the outer zone, the vapor density decreases. Particle formation and growth is most important at the inner front and inside the intermediate zone. This consumes the supply of metal vapor, causing vapor density to drop progressively through the intermediate zone. The vapor that eventually reaches the outer zone is dilute, and cool, and only a few smaller clusters grow in this region.

ACKNOWLEDGMENTS

The authors are grateful to G. Torchet and P. A. Buffat for valuable discussions related to this work, and to the staff at the CIME of EPFL for their support in carrying out the electron microscopy studies. This research has been supported financially by the Swiss National Science Foundation (FNRS).

*Present address: Dépertement des matériaux, EPFL, 1015 Lausanne, Switzerland.

†Author to whom correspondence should be addressed.

[1] S. Ino, J. Phys. Soc. Jpn. **21**, 346 (1966); S. Ino and D. Ogawa, *ibid*. **22**, 1365 (1967); J. G. Allpress and J. V. Sanders, Surf. Sci. **7**, 1 (1967).

[2] A. Howie and L. D. Marks, Philos. Mag. A **49**, 95 (1984).

[3] S. Ino, J. Phys. Soc. Jpn. **27**, 941 (1969).

[4] F. Ercolessi, W. Andreoni, and E. Tosatti, Phys. Rev. Lett. **66**, 911 (1991).

[5] J. Uppenbrink and D. J. Wales, J. Chem. Phys. **96**, 8520 (1992).

[6] S. Valkealahti and M. Manninen, Phys. Rev. B **45**, 9459 (1992).

[7] C. L. Cleveland and U. Landman, J. Chem. Phys. **94**, 7376 (1991).

[8] J. Farges, M.-F. de Feraudy, B. Raoult, and G. Torchet, Acta Crystallogr. A **38**, 656 (1982).

[9] B. Raoult, J. Farges, M.-F. de Feraudy, and G. Torchet, Philos. Mag. B **60**, 881 (1989).

[10] L. D. Marks, Rep. Prog. Phys. **57**, 603 (1994).

[11] P. M. Ajayan and L. D. Marks, Phys. Rev. Lett. **60**, 585 (1988).

[12] N. Doraiswamy and L. D. Marks, Philos. Mag. B **71**, 291 (1995).

[13] P. Audit, J. Phys. (Paris) **30**, 192 (1969).

[14] A. Yokozeki and G. D. Stein, J. Appl. Phys. **49**, 2224 (1978); B. G. be Boer and G. D. Stein, Surf. Sci. **106**, 84 (1981).

[15] J. Farges, M.-F. de Feraudy, B. Raoult, and G. Torchet, J. Chem. Phys. **84**, 3491 (1986).

[16] B. W. van de Waal, Phys. Rev. Lett. **76**, 1083 (1996).

[17] S. A. Nepijko, V. I. Styopkin, H. Hofmeister, and R. Scholtz, J. Cryst. Growth **76**, 501 (1986).

[18] K. Heinemann, M. J. Yacamán, C. Y. Yang, and H. Poppa, J. Cryst. Growth **47**, 177 (1979); M. J. Yacamán, K. Heinemann, C. Y. Yang, and H. Poppa, *ibid*. **47**, 187 (1979); P. Schabes-Retchkiman, A. Gómez, G. Vázquez-Polo, and M. J. Yacamán, J. Vac. Sci. Technol. A **2**, 22 (1983).

[19] B. W. van de Waal, J. Chem. Phys. **98**, 4909 (1993).

[20] D. Ugarte, Electron Microscopy **2**, 677 (1992).

[21] M. Flüeli, P.-A. Buffat, and J.-P. Borel, Surf. Sci. **202**, 343 (1988).

[22] B. D. Hall, M. Flüeli, D. Reinhard, J.-P. Borel, and R. Monot, Rev. Sci. Instrum. **62**, 1481 (1991).

[23] P.-A. Buffat, M. Flüeli, R. Spycher, P. Stadelmann, and J.-P. Borel, Faraday Discuss. **92**, 173 (1991).

[24] B. D. Hall, M. Flüeli, R. Monot, and J.-P. Borel, Phys. Rev. B **43**, 3906 (1991).

[25] A. L. Mackay, Acta Crystallogr. **15**, 916 (1962).

[26] B. D. Hall, D. Ugarte, D. Reinhard, and R. Monot, J. Chem. Phys. **103**, 2384 (1995).

[27] T. B. Rymer, *Electron Diffraction* (Chapman and Hall, London, 1970), Chap. 8.

[28] P. A. Doyle and P. S. Turner, Acta Crystallogr. A **24**, 390 (1967).

[29] B. D. Hall and R. Monot, Comput. Phys. **5**, 414 (1991).

[30] B. G. Bagley, Nature **208**, 674 (1965).

[31] In previous experiments on unsupported silver clusters, in which much smaller particles were produced, temperature and gas pressures were lower. The growth of clusters in these experiments was satisfactorily explained by thermodynamic considerations (Ref. 24).

[32] E. Gillet and M. Gillet, J. Cryst. Growth **13/14**, 212 (1972).

[33] M. Gillet, J. Cryst. Growth **36**, 239 (1976).

[34] J. J. Métois, G. D. T. Spiller, and J. A. Venables, Philos. Mag. **46**, 1015 (1982).

[35] L. D. Marks, Philos. Mag. A **49**, 81 (1984).

[36] J. G. Allpress and J. V. Sanders, Surf. Sci. **7**, 1 (1967).

[37] L. L. Boyer and J. Q. Broughton, Phys. Rev. B **42**, 11 461 (1990).

[38] J. A. Northby, J. Chem. Phys. **87**, 6166 (1987).

[39] N. Wada, Jpn. J. Appl. Phys. **6**, 553 (1967); **7**, 1287 (1968).

[40] T. Hayashi, T. Ohno, S. Yatsuya, and R. Uyeda, Jpn. J. Appl. Phys. **16**, 705 (1977).

[41] C. G. Granquist and R. A. Buhrman, J. Appl. Phys. **47**, 2200 (1976).

[42] C. Y. Yang, J. Cryst. Growth **47**, 274 (1979).

[43] F. L. Galeener and M. M. Rondoni, *Amorphous and Liquid Semiconductors*, edited by J. Stuke and W. Brenig (Taylor and Francis, London, 1974).

[44] F. Betts and A. Bienenstock, J. Appl. Phys. **43**, 4591 (1972).

[45] D. Reinhard, P. Berthoud, B. D. Hall, S. Valkealahti, and R. Monot (unpublished).

[46] S. Valkealahti (private communication).

[47] F. Ercolessi (private communication).

[48] H. S. Lim, C. K. Ong, and F. Ercolessi, Surf. Sci. **269/270**, 1109 (1992).

[49] H. Abe, W. Schulze, and B. Tesche, Chem. Phys. **47**, 95 (1980); W. Schulze, F. Frank, K.-P. Charlé, and B. Tesche, Ber. Bunsenges. Phys. Chem. **88**, 263 (1984).

[50] S. Yatsuya, S. Kasukabe, and R. Uyeda, J. Cryst. Growth **24/25**, 319 (1974).

[51] A. Roth, *Vacuum Technology* (North-Holland, Amsterdam, 1982).